ACS APPLIED POLYMER MATERIALS

pubs.acs.org/acsapm
Article

Highly Flexible Strain Sensors Based on CNT-Reinforced Ecoflex Silicone Rubber for Wireless Facemask Breathing Monitoring via Bluetooth

Antonio del Bosque,* Xoan Xosé Fernández Sánchez-Romate, Álvaro De La Llana Calvo, Pedro Rafael Fernández, Susana Borromeo, María Sánchez, and Alejandro Ureña

Cite This: ACS Appl. Polym. Mater. 2023, 5, 8589−8599
Read Online

ABSTRACT: Highly stretchable strain sensors based on carbon nanotube (CNT)-reinforced Ecoflex silicone rubber are developed for breathing monitoring purposes. The addition of CNTs promotes an improvement in electrical conductivity and mechanical properties (Young's modulus and tensile strength) due to its good dispersion in Ecoflex. The evaluation of strain monitoring response, in both tensile and compression conditions, indicates a wide strain detection range and an ultrasensitive response at high strain levels, reaching a gauge factor of around 10^4 at 70% or 10^5 at 300% for 0.3 and 0.7 wt % CNT-reinforced sensors, respectively. They show a quite stable electrical response under 2000 cycling loads and different levels of frequencies. Moreover, the response and recovery times are in the range of milliseconds (∼600 and ∼800 ms, respectively). Finally, a proof-of-concept of wireless facemask breathing monitoring was carried out with Bluetooth Low Energy technology and a platform that has been developed to acquire, filter, visualize, and store the breathing signal. With this, the respiration rate can be unequivocally monitored as well as the difference between inspiration and expiration. Thus, this type of trial is proposed for breath monitoring in medical analysis, emergency teams, or first aid.

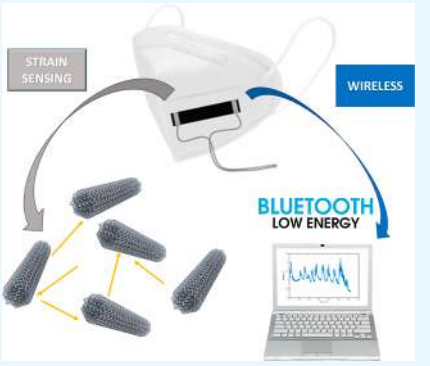

KEYWORDS: *carbon nanotubes, breathing monitoring, Ecoflex, Bluetooth Low Energy, nanocomposites*

INTRODUCTION

Nowadays, there is an increasing interest in the development of wearable devices for strain monitoring purposes. Among others, stretchable strain sensors based on nanocomposites, that is, polymers reinforced with nanoparticles, often show improved sensitivity, resolution, reduced weight, cost-effectiveness, and accuracy compared to conventional sensors.[1] This makes them ideal for use in a variety of applications, including human motion monitoring,[2] structural health monitoring,[3] or soft robotics.[4,5]

Furthermore, due to the COVID-19 pandemic, people are increasingly interested in real-time monitoring of their physiological indicators such as pulse, blood pressure, heartbeat, and breath.[6] As a result, the ability to accurately detect these indicators has become a crucial feature in current smart health monitoring devices. More specifically, there are respiratory illnesses such as tonsillitis, the common cold, influenza, pneumonia, asthma, etc., where medical managers desire to monitor human respiration remotely to assess the development of the disease. Flexible wearable sensors, which are a key component of these devices, have become a focus of research in the field of strain sensing.

Among the wide range of nanofillers that can be used to manufacture wearable strain sensors, carbon nanotubes (CNTs) are very promising because they can greatly enhance the electrical conductivity of an insulating polymer when added to it in a relatively small proportion in comparison with other alternatives such as graphene nanoplatelets (GNPs) or carbon black (CB).[7−9] CNTs can generate an electrical percolation network that is very sensitive to strain, causing changes in the overall electrical conductivity due to the creation or breakage of conductive pathways when the material is subjected to a strain field. More precisely, the strain of the doped polymer promotes changes in the distances between conductive neighboring nanoparticles, which have a very sensitive effect on tunneling conduction mechanisms.[10] This property allows CNT-based sensors to detect strain by measuring changes in their electrical conductivities.[11] Several methods can be used to manufacture CNT-doped flexible polymer strain sensors, including solvent casting,[12] melt blending,[13] and in situ polymerization.[14] Each of these

Received: July 26, 2023
Accepted: August 10, 2023
Published: September 5, 2023

https://doi.org/10.1021/acsapm.3c01689
ACS Appl. Polym. Mater. 2023, 5, 8589−8599

methods has its advantages and disadvantages, and the optimal method will depend on the specific application.[15]

Different silicone elastomers are used for developing CNT-doped wearable strain sensors, such as homemade silicone,[16] Ecoflex,[17,18] or PDMS.[19−23] On the one hand, PDMS is commonly used due to its high Poisson ratio (∼0.5), which increases the sensitivity by promoting a higher interparticle variation when applying a strain level. However, the high Young's modulus (between 0.4 and 3.5 MPa) in its stoichiometric ratio[24] can make it difficult to adhere on devices or skin. In comparison, the Ecoflex polymer has a lower elastic modulus (typically between 100 and 125 kPa) and higher elongation at failure,[25] making it more suitable for attachable strain sensor applications.[26] In addition, it is a good alternative that would not promote a significant increase in the cost of the sensor due to the commercial availability of the Ecoflex rubber.

Given the state of the art, there are smart masks that are able to detect CO_2 levels, breathing, or body temperature with different sensors,[27−31] but these are heavy and have great limitations for the comfort of the person who uses them. Another strategy to detect respiration is based on monitoring the humidity caused by inspiration/expiration, where extensive work has been done on nanocomposite-based humidity sensors.[32−35] Moreover, there are some superficial proofs-of-concept with an attached nanocomposite in the mask,[6,36] but the signal is not remotely monitored. Nowadays, there is no cheap, wearable, and integrated solution to monitor the breathing of patients wirelessly.

The purpose of this study is to design a CNT−Ecoflex polymer wearable strain sensor for wireless monitoring of breathing through a mask by using wireless technology. Thus, the respiration rate can be recorded due to the strain changes that occur in the mask, with a sensor glued to the outside of the mask. The first step in this process involves conducting an electrical and electromechanical study to determine the optimal conditions for maximum sensitivity under tensile and compression conditions. Next, the robustness of the electrical response to tensile cycling loads is evaluated. Finally, the optimized sensor is placed in a mask to test its ability to monitor human breath. To verify the results, an acquisition and processing electronics board has been developed to send the signal wirelessly.

EXPERIMENTAL METHODS

Materials. The sensors were based on a CNT-reinforced silicone elastomer. The silicone elastomer Ecoflex 00-30 was provided by *Smooth-On*, as a two-component system (part A and part B), which is constituted by equal-mixing and platinum-catalyzed, 3000 mPa·s being its room-temperature viscosity. Multi-walled CNTs NC7000 were supplied by *Nanocyl*, having a surface area of 250−300 m^2/g, an average diameter of 9.5 nm, and a length of up to 1.5 μm with 90% carbon purity.

Manufacturing of CNT-Reinforced Ecoflex Sensors. Ecoflex nanocomposites were manufactured dispersing 0.1, 0.2, 0.3, 0.5, and 0.7 wt % CNT contents by a three-roll-milling procedure in a mini-calendar *EKATK 80*. These contents were chosen to explore the percolation threshold of the system and the electromechanical behavior under tensile and compression loads.

First, CNTs were added separately to Ecoflex parts (A and B) and manually mechanically mixed by hand for 2 min. After this, the dispersion stage by a three-roll-milling process was carried out. The process consisted of passing the CNT−Ecoflex mixture through three adjacent rollers rotating in opposite directions and at different speeds with a progressive reduction of the gaps between subsequent rollers. Here, the shear forces applied as the mixture flows through the rollers promote the breakage of CNT agglomerates, and thus, their dispersion in the Ecoflex matrix was achieved. Finally, the mixture was collected by a blade system after the third roll. The calendaring parameters were previously optimized[37] and are listed in Table 1.

Table 1. Process Conditions for the Calendaring Dispersion at Room Temperature

cycle	first gap (μm)	last gap (μm)	roll	velocity (rpm)
1	120	40	**1**	28
2	75	25	**2**	125
3	45	15	**3**	250
4−7	15	5		

Next, each mixture was heated to 80 °C and placed under vacuum conditions for 20 min to remove the bubbles that had been trapped during the dispersion process. Then, both doped parts were manually mixed for 2 min. The mixture was then poured in a mold with the final geometry of the samples that had been treated with a layer of a poly(vinyl alcohol)-based release agent. Finally, the system was cured at room temperature for 1 day, which is one of the curing cycles indicated in the Ecoflex data sheet.

Characterization. *Analysis of CNT Distribution.* *Nikon Coolpix 990* light transmission optical microscopy (TOM) was used to study the CNT distribution just after the calendaring procedure and before the curing stage by placing a drop of the mixture between two mica crystals. In addition, *ImageJ* software was used to analyze the average size of the aggregates from the TOM images.

Electrical Conductivity Measurements. DC electrical conductivity was evaluated by using a *Keithley 2410* source meter unit. The current carried was measured by applying different constant voltages, from −20 to 20 V, using at least three specimens of 60 × 18 × 5 mm^3 dimensions. The electrical resistance was calculated by measuring the slope of the current−voltage curve. For the experiments, four copper electrodes were attached to the nanocomposite specimen by using conductive silver ink to perform a four-probe measurement, as shown in Figure 1a.

Electromechanical Tests. The electromechanical behavior of the nanocomposites was evaluated under tensile and compression loads using a *ZwickRoell Z100* universal tensile machine. At least three specimens of each condition were tested using a 500 N load cell. In this regard, tensile tests were performed following ISO 527-1:2020 at a test rate of 40 mm/min and a preload of 0.5 N, while compression tests were carried out on specimens with dimensions 15 × 15 × 10 mm^3, at a test rate of 5 mm/min, a preload of 1 N, and up to a strain level of 0.45 mm/mm.

Simultaneously with the mechanical test, electrical characterization was carried out by monitoring the electrical resistance changes of the specimens between two electrodes. An *Agilent DAQ970A* data acquisition system with a *DAQM902A* module was used for this purpose. Figure 1b shows the arrangement of copper wire electrodes attached with silver ink to the nanocomposites. In addition, the samples were electrically isolated from the metallic grips by the application of an adhesive layer. The strain sensitivity or gauge factor (GF) was calculated at different strain levels for tensile and compression loads and was obtained by dividing the normalized electrical resistance by the applied strain, as shown in eq 1

$$\mathrm{GF} = \frac{\Delta R/R_0}{\varepsilon} \tag{1}$$

where R_0 is the initial electrical resistance, ε is the applied strain on the sample, and ΔR is the instantaneous electrical resistance increment at the initial electrical resistance.

The hysteresis was evaluated after a loading and unloading cycle up to 40% strain and at the test rate of 40 mm/min (same as previously mentioned). The long-term stability of the optimized sensor (0.3 wt % CNT) was evaluated by recording the electrical response over 2000 tensile cycles up to 5 and 60% strain levels at a fixed rate of 50 mm/

https://doi.org/10.1021/acsapm.3c01689
ACS Appl. Polym. Mater. 2023, 5, 8589−8599

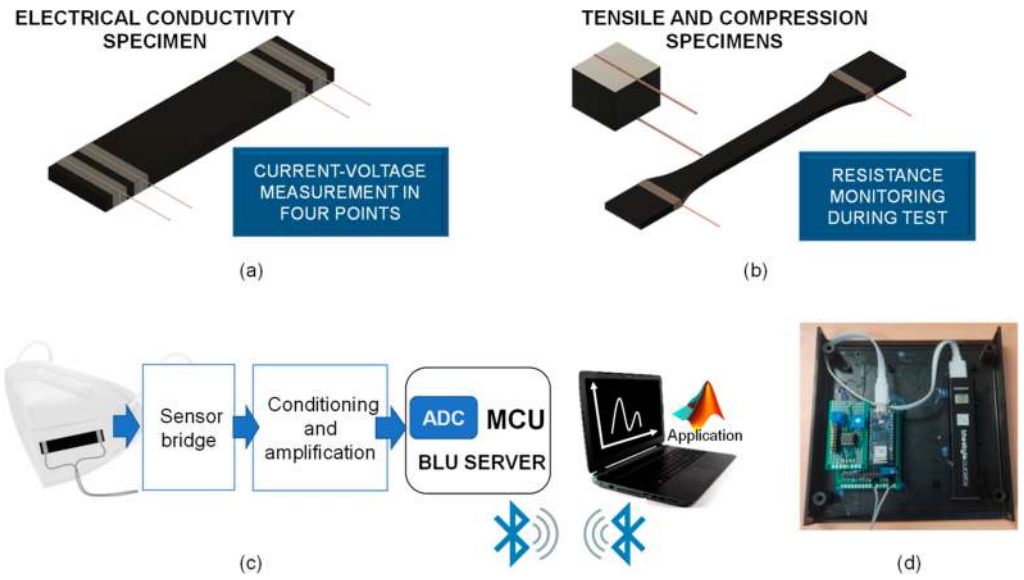

Figure 1. CNT−Ecoflex specimens and electrode disposition in (a) electrical conductivity and (b) tensile/compression tests. (c) Scheme of wireless facemask breathing monitoring via Bluetooth connection and a (d) real electronic panel.

min. Furthermore, the behavior of the electrical response under different tensile frequencies (10, 20, 30, 50, and 100 mm/min) was studied in 5 tensile cycles. The transient response of the optimized sensor was evaluated in terms of response and recovery times, which were analyzed by applying a 2% strain level to the sensor for 10 s and then recovering the initial position at the same rate. In this case, the strain rate for the stretch and recovery was 200 mm/min.

Temperature Test. The DC electrical resistance was measured, while the conductive nanocomposites were subjected to a temperature variation in an oven, from 30 to 100 °C. It was measured by using the same multimeter as mentioned in the previous section.

Wireless Facemask Breathing Monitoring. A human respiration detection test was performed by placing the optimized sensor with dimensions of 30 × 3 × 1.5 mm^3 in a conventional mask (FFP2), as shown in Figure 1c. Electrodes were placed at the ends of the sensor and fixed with silver ink and an adhesive layer. The sensor was placed on one side of the mask. This causes variations in its resistance value above its nominal value due to the strain produced in the mask by the breath stresses.

To capture and process the signal, a microcontroller-based acquisition system was designed and implemented, including a Bluetooth Low Energy (BLE) interface. The system was composed of two interconnected cards (Figure 1c): the first one was the signal conditioning circuit containing all of the elements coming from the sensor and the second one contained the embedded system and wireless communication block.

The first stages of signal sensing and conditioning corresponded to a classic structure consisting of a Wheatstone bridge, an instrumental amplifier, and a low-pass filter. The analogue input range supported was between 0 and 3.3 V. The designed circuit included different potentiometric adjustment elements that allowed calibration of the output voltage of the bridge, the gain, and the output offset of the instrumental amplifier. The output signal was delivered to a microcontroller in charge of both the signal digitization process and the wireless communication to a PC.

Since the objective was to measure resistance variations, a Wheatstone bridge was used in the first stage. This configuration allows detecting very weak variations of the sensor resistance due to the low strain levels that human breathing promoted in the mask. The rest of the resistors had the same value as that of the sensor in the resting state. This design rule was followed to obtain the highest sensitivity of the system. Thus, variations of R for R_0 were converted into an electrical signal (potential difference) that followed the human breathing.

Once the analogue signal was amplified, it was necessary to digitize it for data transmission and recording. For this purpose, the analogue-to-digital converter included in the MCU (microcontroller unit) was used. The analogue input range supported was 0 to 3.3 V; i.e., the input signal to the ADC (analog-to-digital converter), delivered by the instrumentation amplifier, had to have that range of variation. For this purpose, the gain of the amplifier could be adjusted by means of a potentiometer.

Considering that the input signal had very low-frequency components (<1 Hz), the sampling, signal range, and latency requirements demanded by the system were easily met by many commercially available integrated systems (Figure 1d). The selected MCU operated at 3.3 V and included a 32-bit *Arm Cortex-M0 SAMD21G18A* processor (48 MHz). A *u-blox NINA-W102* module was also added to ensure the BLE connectivity. BLE enables communication between devices and operates at 2.4 GHz (industrial, scientific, and medical band), allowing a maximum transfer rate of approximately 1 Mbps. It uses Advanced Encryption Standard encryption and configurable security. This module grants a range of 10−15 m, which is not a minor problem when the signal in question shares the wireless channel with several devices. The ADC can process variables using a tunable resolution of 8, 10, to 12 bits. Once the signal was digitized, the MCU sent the signal through the BLE interface. The use of BLE was chosen because it had, among others, the following advantages: the power required was very low, the coverage and sending speeds were more than sufficient for the application, and it had high compatibility with many other systems such as the most current mobile devices. The receiver used was a PC with Bluetooth connectivity. A *Matlab* application was developed to visualize and process the signals in real-time. The data were visualized and stored in files for further study through a user-friendly interface.

In this regard, our system was oversized to meet these requirements so that it can be used in other conditions or future applications. It was ensured that the signal of interest can be sampled up to a maximum of 180 samples per second, being sufficient for the respiration signal under different conditions (12−20 breaths per minute).

RESULTS AND DISCUSSION

The electrical and electromechanical properties of the CNT−Ecoflex nanocomposites were tested under tensile and compression conditions. Next, the sensor with the highest strain sensitivity was subjected to consecutive load cycling to demonstrate its robustness and stability. Finally, a test was

https://doi.org/10.1021/acsapm.3c01689
ACS Appl. Polym. Mater. 2023, 5, 8589−8599

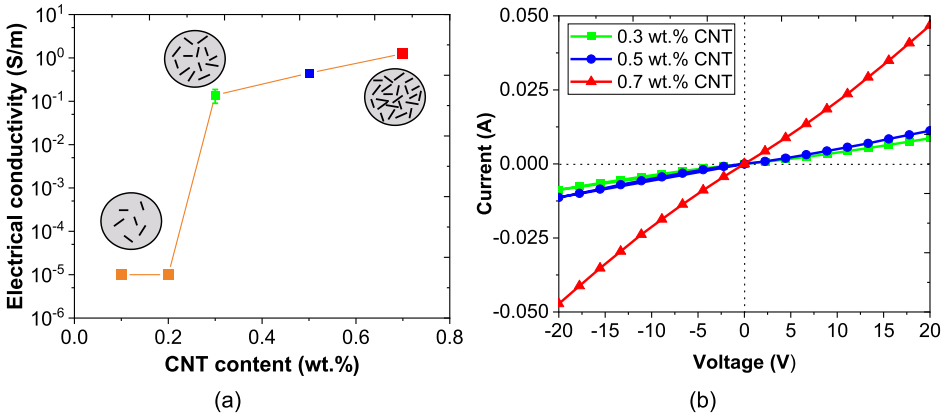

Figure 2. (a) Electrical conductivity measurements and (b) *I*−*V* curves for the CNT−Ecoflex nanocomposites.

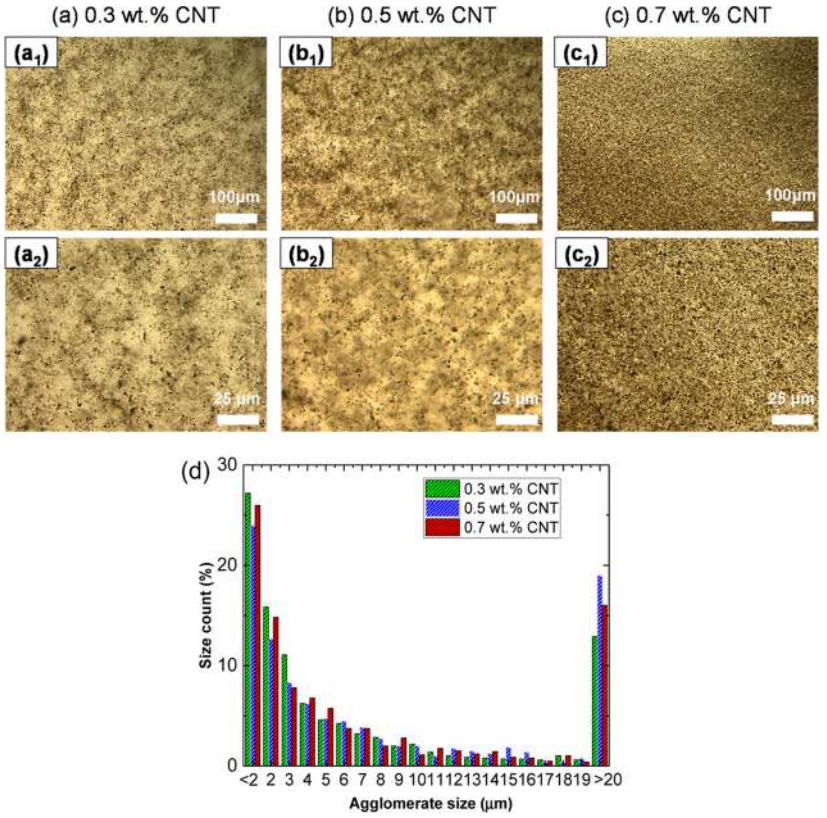

Figure 3. TOM images of the electrically conductive CNT−Ecoflex dispersions achieved before the curing step in (a) 0.3, (b) 0.5, and (c) 0.7 wt % CNT nanocomposites. (d) Histogram of agglomerate size for the different conditions.

performed to wirelessly monitor human respiration using the optimized sensor placed in a mask and connected via a BLE interface.

Electrical Conductivity Study of CNT−Ecoflex Nanocomposites. Figure 2a summarizes the electrical conductivities measured for the different CNT contents tested for the fabricated nanocomposites. It can be observed that the samples with less than 0.3 wt % CNTs are below the threshold of the measurement device (10^{-5} S/m), so they can be considered as electrically nonconductive, and therefore, the percolation threshold is determined between 0.2 and 0.3 wt % CNT. At higher contents, an increase of the electrical conductivity is observed when increasing nanoparticle content, as expected, due to a higher number of electrical pathways present in the network. In all cases, the current−voltage response was observed to be linear (Figure 2b), denoting ohmic behavior. Furthermore, the electrical conductivity values were in a similar range to those found in previous studies using other commercial silicone elastomers,[38] demonstrating the dispersion effectiveness of the three-roll-milling method.

The effectiveness of the three-roll-milling method in achieving a homogeneous dispersion can be observed in the CNT distribution by TOM analysis of the CNT−Ecoflex droplets. Here, it can be observed that the CNTs are well-dispersed throughout the material in each conductive condition (Figure 3a−c), without the presence of prevalent CNT aggregates. More specifically, from these images, it is possible to quantify the average size of the aggregates, the results of which are summarized in Figure 3d. Here, it can be observed that the size distribution of the CNT aggregates does

https://doi.org/10.1021/acsapm.3c01689
ACS Appl. Polym. Mater. 2023, 5, 8589−8599

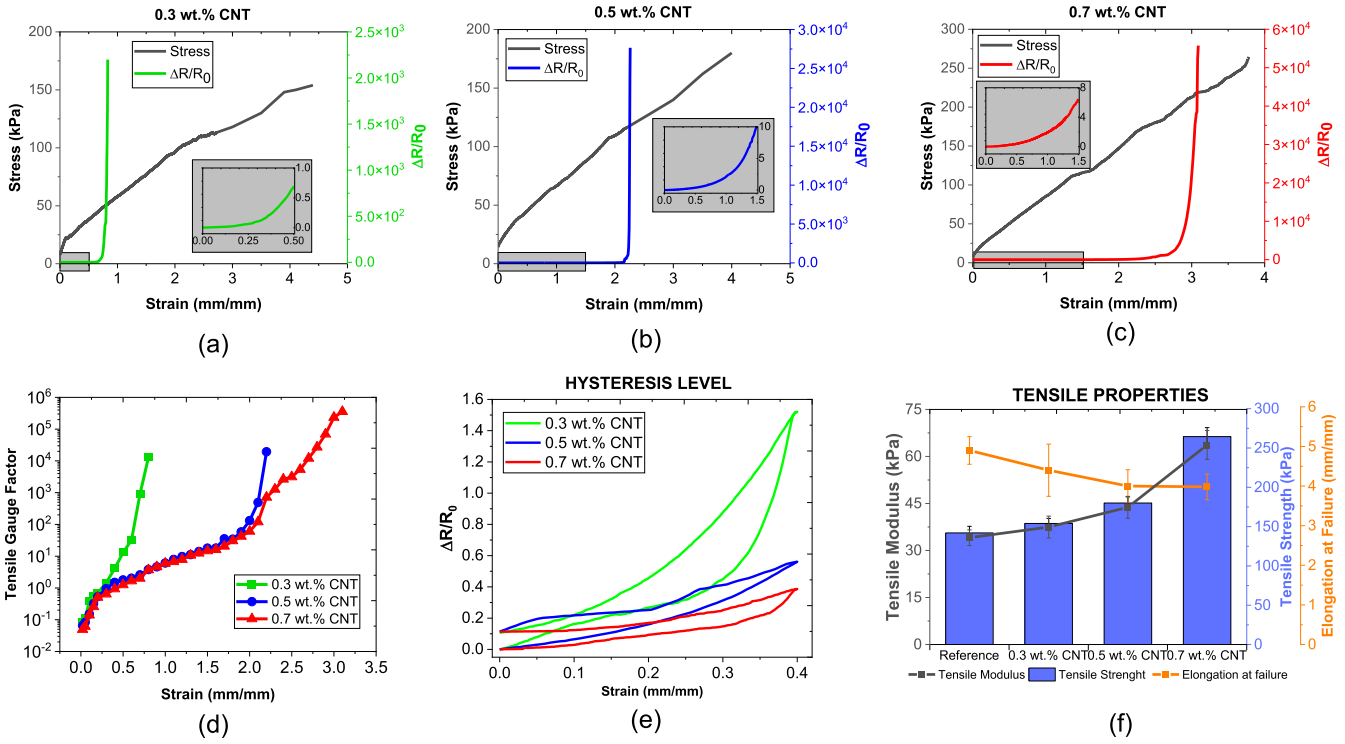

Figure 4. Tensile electromechanical curves of (a) 0.3, (b) 0.5, and (c) 0.7 wt % CNT-reinforced Ecoflex. (d) GF, (e) hysteresis level, and (f) mechanical properties as a function of CNT content in the tensile mode of the developed nanocomposites.

not significantly vary between tested conditions (only a slight increase in the proportion of larger aggregates with increasing CNT content). Therefore, it can be concluded that the effectiveness of the three-roll-milling process is quite high and, thus, would explain the continuous increase of electrical conductivity with CNT content, not reaching saturation values at the highest content (0.7 wt %). Moreover, it is well-known that, at very low CNT contents, the efficiency of the three-roll-milling method may be significantly lower, with the presence of more isolated CNT regions and nonpercolated areas (Figure 3a and b),[39] whereas at higher CNT-contents, the increasing viscosity can promote a more aggressive breakage of CNT aggregates.

Quasi-Static Electromechanical Study of CNT−Ecoflex Sensors. The electromechanical response under quasi-static load conditions, both tensile and compressive, is analyzed to better understand the electrical sensitivity of the proposed sensors.

Tensile Mode. Figure 4 shows the electromechanical behavior and mechanical characteristics of the CNT−Ecoflex samples under quasi-static tensile loading.

First, a linear-exponential correlation is observed between the applied strain and the electrical resistance measured for every condition (Figure 4a−c). This linear-exponential correlation is explained by the predominance of tunneling mechanisms over the contact and intrinsic ones. It is well-known that this tunneling transport follows a linear-exponential correlation with the interparticle distance, according to Simmons' expression.[40] This exponential behavior is more prevalent with decreasing CNT content due to the higher dominance of the tunneling mechanisms under these conditions. More specifically, the GF increases more drastically for samples with 0.3 wt % CNT than for those with 0.7% wt % CNT, as shown in the plot of Figure 4d. In this case, although the GF at low strains is relatively small, the sensors are able to monitor a much wider range of strain levels than other sensors based on GNPs, where the loss of the electrical conductivity is achieved at much smaller strain levels.[19,41] However, the GF reached at high strain levels is around 10^4 at 70% for 0.3 wt % CNT or 10^5 at 300% for 0.7 wt % CNT sensors. Hysteresis was evaluated after a loading and unloading cycle of up to 40% strain and at the same speed as the tensile tests indicated, as indicated in Figure 4e. The developed sensors show some level of hysteresis, explained by the viscoelasticity of the matrix.

Furthermore, the CNT addition does not only provide electrical conductivity to the Ecoflex insulating hosting matrix but also has a significant effect on the mechanical properties of the system. Specifically, there is an increase of both Young's modulus and tensile strength with CNT content (Figure 4f) due to the reinforcing effect of the CNTs. In fact, the increase of both strength and stiffness is an indicator of a good distribution of CNTs.[42] Moreover, the elongation at break slightly decreases with CNT content, but the values are well above those found for other flexible strain sensors.[19,38]

Figure 5 shows the GF value and maximum working strain range of the developed nanocomposites compared to those of other carbon-based flexible strain sensors reported in the literature. The comparison is made with a wide range of flexible polymers (PDMS, Ecoflex, TPU, or IR) doped with carbon nanoparticles (CNT, CB, and graphene).[19,21,38,43−53] Most of these sensors cannot satisfy the requirements of a high GF and large strain range simultaneously, while nanocomposites obtained in this work stand out. As discussed above, the GF value of developed sensors consistently increases within the entire strain range, indicating that the conductive network is not completely disconnected, making it potentially useful for practical applications.

https://doi.org/10.1021/acsapm.3c01689
ACS Appl. Polym. Mater. 2023, 5, 8589−8599

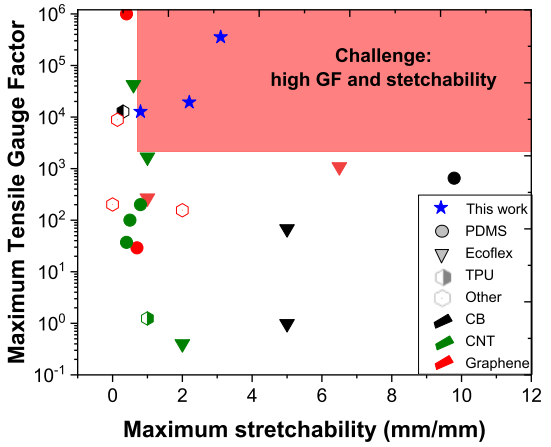

Figure 5. Comparison of the maximum tensile GF reached at the maximum strain level of developed strain sensors in the literature.

Compression Mode. Figure 6 shows the electromechanical behavior and mechanical properties of the CNT−Ecoflex nanocomposites under compression loading.

It can be observed that the electrical response also follows a linear-exponential trend as a function of applied strain (Figure 6a−c), as was also observed in tensile tests, due to the prevalence of tunneling transport mechanisms. However, many differences can be found when compared with the electromechanical behavior at tensile loading. First, and surprisingly, an increase of the electrical resistance is observed under compressive conditions, showing, in this case, a lower GF value. This has been observed in previous studies[19,54] and is correlated to the variation of the geometrical network of the CNTs during the compression. More specifically, the changes in the geometry, even under compressive conditions, can lead to a decrease in contact mechanisms and thus an increase of the electrical resistance.[54] In addition, it can be noticed that the GF values are significantly lower than those in tensile conditions (Figure 6d). This is explained by the mechanisms acting in this case since two prevalent effects can be found: (i) on the one side, a decrease of the electrical resistance due to in-plane effects and (ii) an increase due to the out-of-plane effects, a fact observed previously by Kuronuma et al.[55] The prevalence of out-of-plane or in-plane mechanisms governs the electrical behavior under compressive conditions and thus explains the lower sensitivity under these conditions.

Regarding the mechanical properties, it is observed that the addition of CNTs promotes a significant increase in the compressive modulus (Figure 6e). Here, it can be observed that, by increasing the CNT content, a greater stiffening effect occurs, especially, at high strain levels, due to the reinforcing effect of CNTs that promotes a more efficient load transfer.[56]

Dynamic Electrical Analysis of Optimized CNT−Ecoflex Sensors. Figure 7 shows the electromechanical response to cycling load as well as the response and the recovery times of the CNT−Ecoflex sensor. At this point, it is important to note that only the 0.3 wt % CNT nanoreinforced sensor was tested as it showed the highest values of sensitivity and would therefore be the most appropriate for strain detection purposes.

It can be observed that the proposed sensor presents a fairly stable electrical response under cyclic loading (Figure 7a and b). The electrical response changes more drastically during the first cycles due to the reorganization of the electrical network in the early stages of the dynamic tests, which is more pronounced with the higher strain level because these effects are accentuated. More specifically, this irreversibility during the

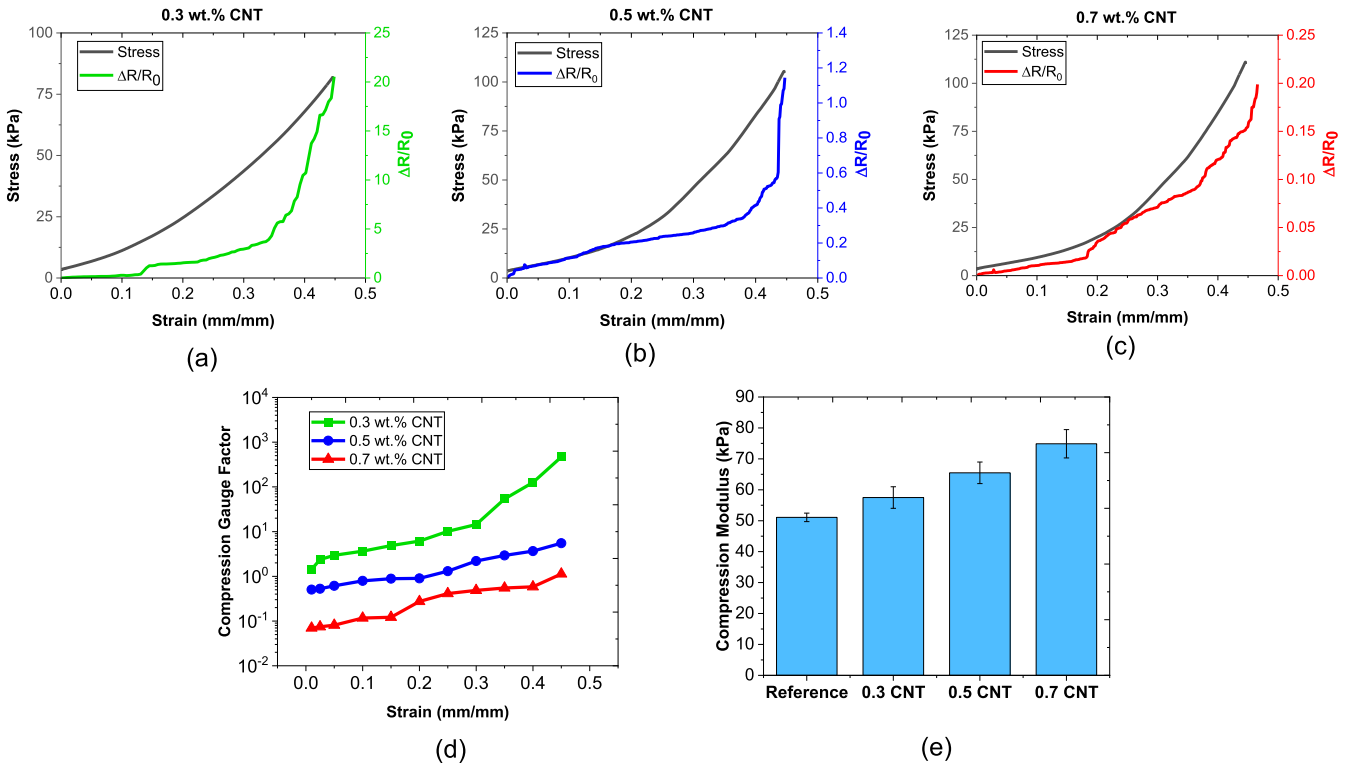

Figure 6. Compression electromechanical curves of (a) 0.3, (b) 0.5, and (c) 0.7 wt % CNT-reinforced Ecoflex. (d) GF and (e) mechanical properties as a function of CNT content in compression mode of the developed nanocomposites.

https://doi.org/10.1021/acsapm.3c01689
ACS Appl. Polym. Mater. 2023, 5, 8589−8599

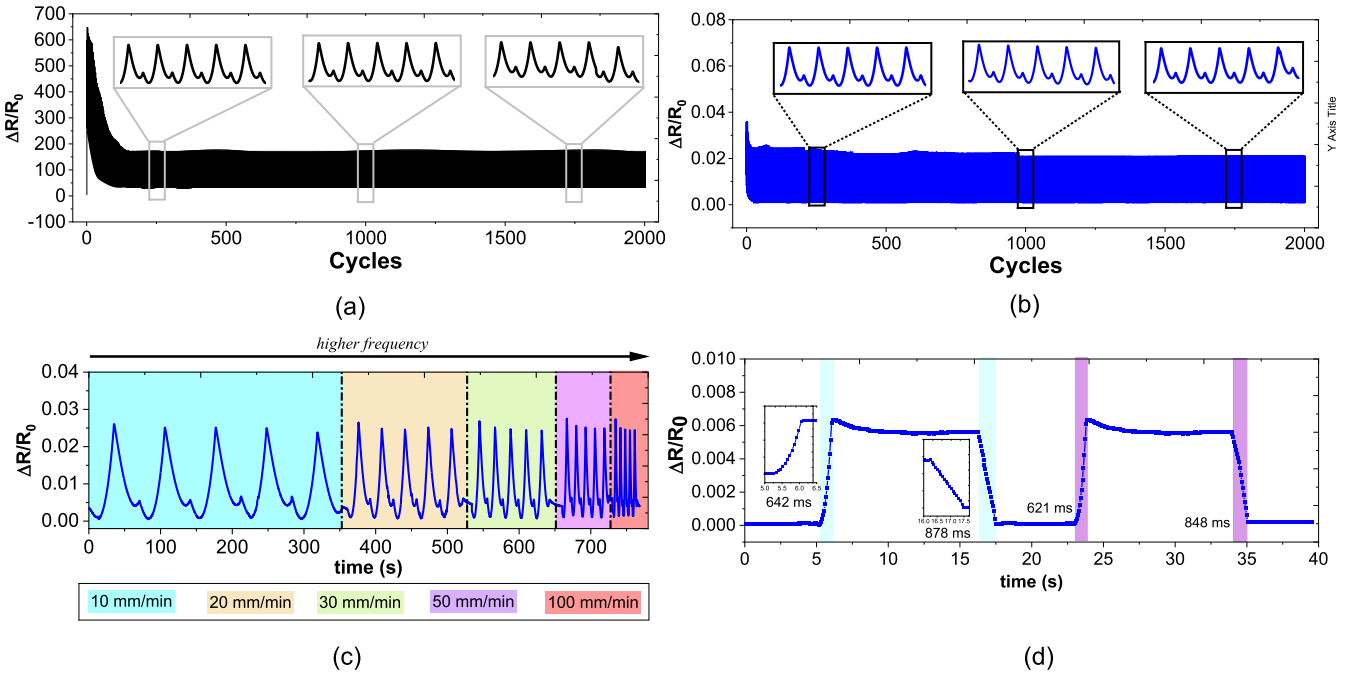

Figure 7. Tensile cycling monitoring of a 0.3 wt % CNT sensor: 2000 cycles at 50 mm/min up to (a) 60 and (b) 5% strain level. (c) 5 cycles up to 5% strain level at 10, 20, 30, 50, and 100 mm/min. (d) Transient response in terms of the response and recovery times for two consecutive cycles.

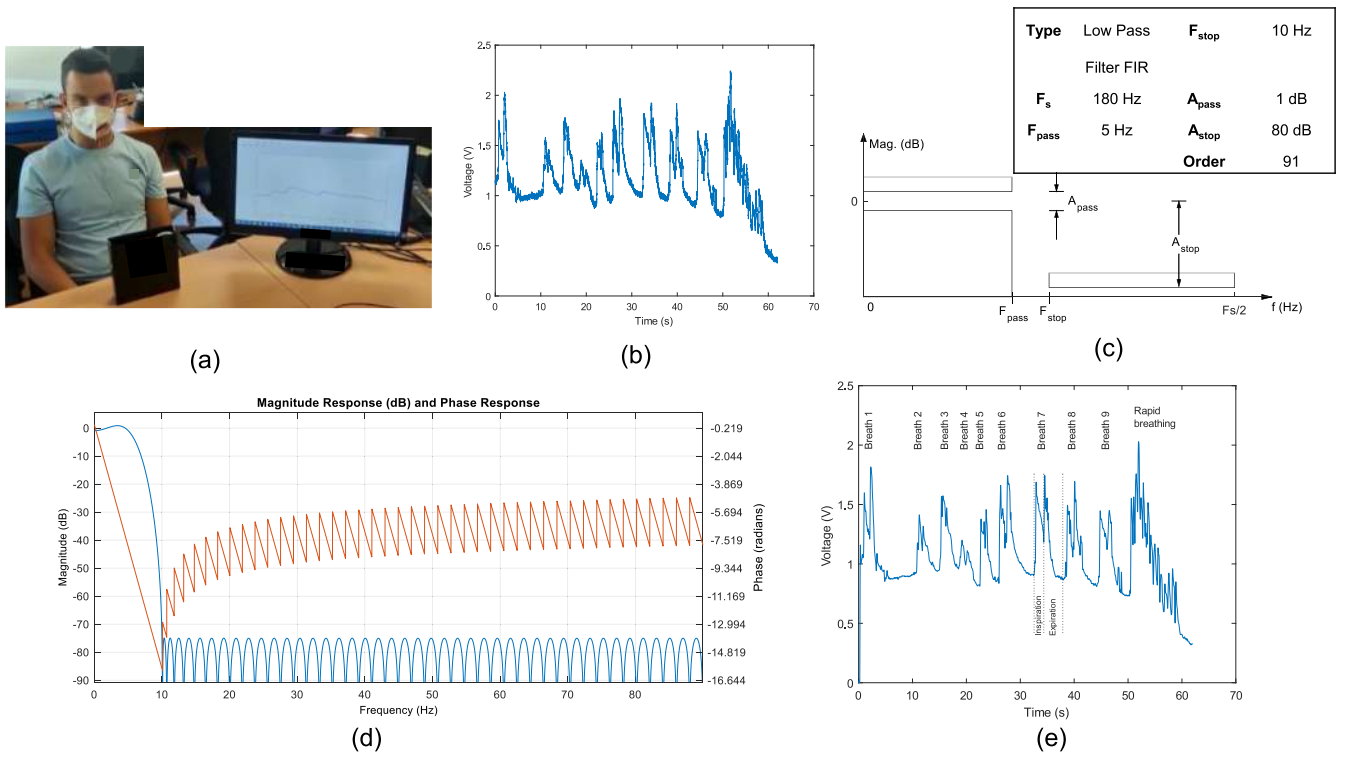

Figure 8. (a) Test scenario and (b) wireless facemask breathing monitoring with raw data received in the application. (c) Digital low pass filter parameters, (d) magnitude (in blue), and phase (in orange) response. (e) Wireless facemask breathing monitoring with the filtered signal.

first few cycles has been widely observed.[57,58] However, as the number of cycles increases, the electrical response stabilizes with no differences prevailing in terms of sensitivity between consecutive cycles (highlighted regions in Figure 7a,b).

Moreover, Figure 7c shows the electrical response under dynamic loading up to 5% strain with variable load frequency. Here, the frequency increases with an increasing test rate. It can be elucidated that the electrical response is in good agreement with the mechanical one, with a similar sensitivity, regardless of the frequency of the dynamic load. Therefore, it can be concluded that the sensor presents a very stable response and a good robustness.

https://doi.org/10.1021/acsapm.3c01689
ACS Appl. Polym. Mater. 2023, 5, 8589−8599

Finally, Figure 7d presents two fundamental parameters to characterize the performance of the sensor: response and recovery times. The first is related to the delay between the applied mechanical force and the electrical response due to the mechanical change. The second is correlated to the delay between the mechanical force when it is withdrawn and the expected electrical response, which would be similar to the initial situation. Therefore, high response and recovery times would denote a greater delay between the mechanical and electrical responses that would negatively affect the performance of the sensor. Here, from analysis of the graphs of Figure 7d, it can be seen that both the response and recovery times are in the millisecond range (~600 and ~800 ms, respectively), which is in good agreement with the response and recovery times obtained for other strain sensors,[59−62] highlighting the applicability of the developed sensors for the detection of strain. Furthermore, when analyzing the electrical response to constant load, it can be observed that it decreases slightly at the first stages of the applied load due to the inherent viscoelastic behavior of the Ecoflex matrix.

Wireless Facemask Breathing Monitoring. Some tests have been performed with the described acquisition and processing system by connecting the optimized sensor (0.3 wt % CNT) attached to the facemask and to the Wheatstone bridge. These tests consisted of a person wearing an FFP2 facemask with the sensor taking several normal and rapid breaths. The different breathing rates cause variations in the strain level in the facemask, which is replicated by the highly flexible sensor. Thus, the sensor generates changes in its electrical resistance. In this regard, it is important to note that the temperature changes produced by breathing do not have a significant impact on the electrical response of the developed sensors, at least up to 60 °C, as shown in Figure S1 of the Supporting Information. On the other hand, the sensor is attached with an adhesive tape on the outside of the facemask, so the humidity that may occur during breathing should not have any influence on the electrical response as these two barriers (the mask fabrics and the adhesive tape) are present. Additionally, in a previous study of a CNT-doped PDMS elastomeric matrix, we demonstrated that hydrothermal aging conditions have no impact on the electrical response of the nanocomposites.[23]

The sensor data, collected by the system, are received wirelessly (BLE) by a computer for further analysis. Figure 8a shows a picture of the test scenario, which is a frame of Video S1 available in the Supporting Information, while Figure 8b indicates the raw data in the application.

A digital filter was implemented to properly analyze the received signal since the respiration information is a low-frequency signal (usually <1 Hz). It is composed of a low-pass filter with the characteristics shown in Figure 8c, where the magnitude and phase response of the filter versus frequency are shown in Figure 8d. The purpose of this processing stage is to remove the high-frequency components due to electronic noise, interferences, etc. The tests were carried out at a high sampling rate (180 samples per second) to show the possibilities of the system. Since the breathing frequency is very low, it is necessary to implement a very restrictive high-order filter, which implies, among other effects, a delay of the output signal of about 300 ms. The optimum solution for this application would be to reduce the sampling frequency by about 20 Hz. Figure 8e shows the results of the signal recorded and filtered in a two-phase experiment: in the first phase, 9 normal breaths are recorded, while in the second phase, a series of rapid breaths are monitored, starting at approximately 53 s. Here, the frequency of breathing and the differences between inspiration and expiration are clearly distinguishable.

The developed system is modular, has low-power consumption, and can be powered by batteries, making it suitable for different wearable applications. For this reason, the proof-of-concept demonstrates the great potential of combining ultrasensitive sensors with adapted electronics for the wireless monitoring of respiration. Therefore, this type of trial is proposed for breath monitoring in medical analysis, emergency teams, or first aid.

CONCLUSIONS

The electromechanical response of highly stretchable sensors for facemask breathing monitoring made of a CNT-reinforced Ecoflex was investigated.

The electrical conductivity analysis shows that the percolation threshold is between 0.2 and 0.3 by weight of CNTs, and an increase in the electrical conductivity is observed with increasing nanoparticle content, considering the good CNT distribution in the Ecoflex matrix at every conductive condition. Moreover, the CNT addition not only provides electrical conductivity to the insulating Ecoflex polymer but also provides an increase of both Young's modulus and tensile strength with CNT content. Thus, the reinforcement effect of CNTs is corroborated due to its good dispersion into the elastomeric matrix.

Evaluation of strain monitoring response, under both tensile and compression loading, indicates low GF values at low strain levels but a wide strain detection range. In this sense, an increase in the CNT content caused a decrease in the sensitivity but an increase in the detection range. For tensile conditions, an ultrasensitive response to high strain levels is observed, reaching a GF of around 10^4 at 70% for 0.3 wt % CNT or 10^5 at 300% for 0.7 wt % CNT sensors.

Regarding the dynamic response of the optimized sensor (0.3 wt % CNT), it shows a fairly stable electrical response after 2000 cycles of variable load and different frequencies. Nevertheless, the electrical response changes more drastically during the first cycles of the dynamic tests due to the reorganization of the electrical network in this stage. Response and recovery times are in the millisecond range (~600 and ~800 ms, respectively).

Finally, a proof-of-concept of wireless monitoring of respiration with a facemask was carried out with BLE technology and a hardware platform that was developed to acquire, visualize, and store the breathing signal. The entire process of acquisition, transmission, and reception of data that allows visualization and identification of different breathing modes was validated. Thus, this type of trial is proposed for breath monitoring in medical analysis, emergency teams, or first aid.

ASSOCIATED CONTENT

Supporting Information

The Supporting Information is available free of charge at https://pubs.acs.org/doi/10.1021/acsapm.3c01689.

Temperature influence in conductive CNT−Ecoflex nanocomposites (PDF)

Wireless facemask breathing monitoring via Bluetooth (MP4)

https://doi.org/10.1021/acsapm.3c01689
ACS Appl. Polym. Mater. 2023, 5, 8589−8599

AUTHOR INFORMATION

Corresponding Author

Antonio del Bosque − *Materials Science and Engineering Area, Escuela Superior de Ciencias Experimentales y Tecnología, Universidad Rey Juan Carlos, 28933 Móstoles, Madrid, Spain;* orcid.org/0000-0002-8301-2159; Phone: +34 914 884 621; Email: antonio.delbosque@urjc.es

Authors

Xoan Xosé Fernández Sánchez-Romate − *Materials Science and Engineering Area, Escuela Superior de Ciencias Experimentales y Tecnología, Universidad Rey Juan Carlos, 28933 Móstoles, Madrid, Spain;* orcid.org/0000-0001-9283-4712

Álvaro De La Llana Calvo − *Electronic Technology Area, Escuela Superior de Ciencias Experimentales y Tecnología, Universidad Rey Juan Carlos, 28933 Móstoles, Madrid, Spain; Electronic Departament, Escuela Politécnica Superior, Universidad de Alcalá, Alcalá de Henares 28801 Madrid, Spain*

Pedro Rafael Fernández − *Electronic Technology Area, Escuela Superior de Ciencias Experimentales y Tecnología, Universidad Rey Juan Carlos, 28933 Móstoles, Madrid, Spain*

Susana Borromeo − *Electronic Technology Area, Escuela Superior de Ciencias Experimentales y Tecnología, Universidad Rey Juan Carlos, 28933 Móstoles, Madrid, Spain;* orcid.org/0000-0002-2353-2902

María Sánchez − *Materials Science and Engineering Area, Escuela Superior de Ciencias Experimentales y Tecnología, Universidad Rey Juan Carlos, 28933 Móstoles, Madrid, Spain*

Alejandro Ureña − *Materials Science and Engineering Area, Escuela Superior de Ciencias Experimentales y Tecnología, Universidad Rey Juan Carlos, 28933 Móstoles, Madrid, Spain*

Complete contact information is available at: https://pubs.acs.org/10.1021/acsapm.3c01689

Author Contributions

The manuscript was written through contributions of all authors. All authors have given approval to the final version of the manuscript.

Notes

The authors declare no competing financial interest.

ACKNOWLEDGMENTS

This work was supported by the Agencia Estatal de Investigación of Spanish Government [project MULTIFUNC−EVs PID2019-107874RB-I00] and Comunidad de Madrid Government [project ADITIMAT-CM (S2018/NMT-4411)].

REFERENCES

(1) Fiorillo, A. S.; Critello, C. D.; Pullano, S. Theory, technology and applications of piezoresistive sensors: A review. *Sens. Actuators, A* **2018**, *281*, 156−175.

(2) Chen, T.; Xie, Y.; Wang, Z.; Lou, J.; Liu, D.; Xu, R.; Cui, Z.; Li, S.; Panahi-Sarmad, M.; Xiao, X. Recent Advances of Flexible Strain Sensors Based on Conductive Fillers and Thermoplastic Polyurethane Matrixes. *ACS Appl. Polym. Mater.* **2021**, *3* (11), 5317−5338.

(3) Sánchez-Romate, X. F.; Moriche, R.; Jiménez-Suárez, A.; Sánchez, M.; Prolongo, S. G.; Güemes, A.; Ureña, A. Highly Sensitive Strain Gauges with Carbon Nanotubes: From Bulk Nanocomposites to Multifunctional Coatings for Damage Sensing. *Appl. Surf. Sci.* **2017**, *424*, 213−221.

(4) Zhang, W.; Zhang, X.; Zhao, W.; Wang, X. High-Sensitivity Composite Dual-Network Hydrogel Strain Sensor and Its Application in Intelligent Recognition and Motion Monitoring. *ACS Appl. Polym. Mater.* **2023**, *5*, 2628−2638.

(5) Gao, Y.; Li, Q.; Wu, R.; Sha, J.; Lu, Y.; Xuan, F. Laser Direct Writing of Ultrahigh Sensitive SiC-Based Strain Sensor Arrays on Elastomer toward Electronic Skins. *Adv. Funct. Mater.* **2019**, *29* (2), 1806786.

(6) Li, C.; Yang, S.; Guo, Y.; Huang, H.; Chen, H.; Zuo, X.; Fan, Z.; Liang, H.; Pan, L. Flexible, Multi-Functional Sensor Based on All-Carbon Sensing Medium with Low Coupling for Ultrahigh-Performance Strain, Temperature and Humidity Sensing. *Chem. Eng. J.* **2021**, *426*, 130364.

(7) Shajari, S.; Mahmoodi, M.; Rajabian, M.; Karan, K.; Sundararaj, U.; Sudak, L. J. Highly Sensitive and Stretchable Carbon Nanotube/Fluoroelastomer Nanocomposite with a Double-Percolated Network for Wearable Electronics. *Adv. Electron. Mater.* **2020**, *6* (2), 1901067.

(8) Han, S.; Wang, P.; Zhou, Y.; Meng, Q.; Aakyiir, M.; Ma, J. Flexible, Mechanically Robust, Multifunctional and Sustainable Cellulose/Graphene Nanocomposite Films for Wearable Human-Motion Monitoring. *Compos. Sci. Technol.* **2022**, *230*, 109451.

(9) Huang, L.; Chen, J.; Xu, Y.; Hu, D.; Cui, X.; Shi, D.; Zhu, Y. Three-Dimensional Light-Weight Piezoresistive Sensors Based on Conductive Polyurethane Sponges Coated with Hybrid CNT/CB Nanoparticles. *Appl. Surf. Sci.* **2021**, *548*, 149268.

(10) Khan, M.; Shah, L. A.; Rahman, T. U.; Yoo, H. M.; Ye, D.; Vacharasin, J. Hydrophobically Associated Functionalized CNT-Reinforced Double-Network Hydrogels as Advanced Flexible Strain Sensors. *ACS Appl. Polym. Mater.* **2022**, *4* (10), 7397−7407.

(11) Akhtar, I.; Chang, S. H. Highly Aligned Carbon Nanotubes and Their Sensor Applications. *Nanoscale* **2020**, *12* (41), 21447−21458.

(12) Wang, X.; Sparkman, J.; Gou, J. Strain Sensing of Printed Carbon Nanotube Sensors on Polyurethane Substrate with Spray Deposition Modeling. *Compos. Commun.* **2017**, *3*, 1−6.

(13) Zhang, Q.; Pan, S.; Ji, C.; Song, J.; Zhang, R.; Zhang, W.; Sang, S. A Shapeable, Ultra-Stretchable Rubber Strain Sensor Based on Carbon Nanotubes and Ag Flakes via Melt-Mixing Process. *J. Mater. Chem. B* **2021**, *9* (16), 3502−3508.

(14) Costa, P.; Carvalho, M. F.; Correia, V.; Viana, J. C.; Lanceros-Mendez, S. Polymer Nanocomposite-Based Strain Sensors with Tailored Processability and Improved Device Integration. *ACS Appl. Nano Mater.* **2018**, *1* (6), 3015−3025.

(15) Kanoun, O.; Bouhamed, A.; Ramalingame, R.; Bautista-Quijano, J. R.; Rajendran, D.; Al-Hamry, A. Review on Conductive Polymer/CNTs Nanocomposites Based Flexible and Stretchable Strain and Pressure Sensors. *Sensors* **2021**, *21* (2), 341.

(16) Cohen, D. J.; Mitra, D.; Peterson, K.; Maharbiz, M. M. A Highly Elastic, Capacitive Strain Gauge Based on Percolating Nanotube Networks. *Nano Lett.* **2012**, *12* (4), 1821−1825.

(17) Lee, J.; Pyo, S.; Kwon, D. S.; Jo, E.; Kim, W.; Kim, J. Ultrasensitive Strain Sensor Based on Separation of Overlapped Carbon Nanotubes. *Small* **2019**, *15* (12), 1805120.

(18) Mai, H.; Mutlu, R.; Tawk, C.; Alici, G.; Sencadas, V. Ultra-Stretchable MWCNT-Ecoflex Piezoresistive Sensors for Human Motion Detection Applications. *Compos. Sci. Technol.* **2019**, *173*, 118−124.

(19) del Bosque, A.; Sánchez-Romate, X. F.; Sánchez, M.; Ureña, A. Ultrasensitive and Highly Stretchable Sensors for Human Motion Monitoring Made of Graphene Reinforced Polydimethylsiloxane: Electromechanical and Complex Impedance Sensing Performance. *Carbon* **2022**, *192*, 234−248.

(20) Lee, J.; Lim, M.; Yoon, J.; Kim, M. S.; Choi, B.; Kim, D. M.; Kim, D. H.; Park, I.; Choi, S. J. Transparent, Flexible Strain Sensor

Based on a Solution-Processed Carbon Nanotube Network. *ACS Appl. Mater. Interfaces* **2017**, *9* (31), 26279−26285.
(21) Gao, Y.; Fang, X.; Tan, J.; Lu, T.; Pan, L.; Xuan, F. Highly Sensitive Strain Sensors Based on Fragmentized Carbon Nanotube/Polydimethylsiloxane Composites. *Nanotechnology* **2018**, *29* (23), 235501.
(22) Chen, J.; Zhu, Y.; Jiang, W. A Stretchable and Transparent Strain Sensor Based on Sandwich-like PDMS/CNTs/PDMS Composite Containing an Ultrathin Conductive CNT Layer. *Compos. Sci. Technol.* **2020**, *186*, 107938.
(23) del Bosque, A.; Sánchez-Romate, X. F.; Calvo, D.; Sánchez, M.; Ureña, A. Mechanical and Sensing Performance under Hydrothermal Ageing of Wearable Sensors Made of Polydimethylsiloxane with Graphitic Nanofillers. *Polym. Degrad. Stab.* **2023**, *209*, 110278.
(24) Johnston, I. D.; McCluskey, D. K.; Tan, C. K. L.; Tracey, M. C.; Allison, S. W.; Sabri, F.; Lai, A.; Altemose, N.; Johnston, I. D.; McCluskey, D. K.; L Tan, C. K.; Tracey, M. C. Mechanical Characterization of Bulk Sylgard 184 for Microfluidics and Microengineering. *J. Micromech. Microeng.* **2014**, *24* (3), 035017.
(25) Liao, Z.; Yang, J.; Hossain, M.; Chagnon, G.; Jing, L.; Yao, X. On the Stress Recovery Behaviour of Ecoflex Silicone Rubbers. *Int. J. Mech. Sci.* **2021**, *206*, 106624.
(26) Herren, B.; Saha, M. C.; Altan, M. C.; Liu, Y. Development of Ultrastretchable and Skin Attachable Nanocomposites for Human Motion Monitoring via Embedded 3D Printing. *Composites, Part B* **2020**, *200*, 108224.
(27) Pan, L.; Wang, C.; Jin, H.; Li, J.; Yang, L.; Zheng, Y.; Wen, Y.; Tan, B. H.; Loh, X. J.; Chen, X. Lab-on-Mask for Remote Respiratory Monitoring. *ACS Mater. Lett.* **2020**, *2* (9), 1178−1181.
(28) Escobedo, P.; Fernández-Ramos, M. D.; López-Ruiz, N.; Moyano-Rodríguez, O.; Martínez-Olmos, A.; Pérez de Vargas-Sansalvador, I. M.; Carvajal, M. A.; Capitán-Vallvey, L. F.; Palma, A. J. Smart Facemask for Wireless CO2Monitoring. *Nat. Commun.* **2022**, *13* (1), 72.
(29) Hyysalo, J.; Dasanayake, S.; Hannu, J.; Schuss, C.; Rajanen, M.; Leppänen, T.; Doermann, D.; Sauvola, J. Smart Mask - Wearable IoT Solution for Improved Protection and Personal Health. *Internet Things* **2022**, *18*, 100511.
(30) Wang, S.; Tai, H.; Liu, B.; Duan, Z.; Yuan, Z.; Pan, H.; Su, Y.; Xie, G.; Du, X.; Jiang, Y. A Facile Respiration-Driven Triboelectric Nanogenerator for Multifunctional Respiratory Monitoring. *Nano Energy* **2019**, *58*, 312−321.
(31) Lou, C.; Hou, K.; Zhu, W.; Wang, X.; Yang, X.; Dong, R.; Chen, H.; Guo, L.; Liu, X. Human Respiratory Monitoring Based on Schottky Resistance Humidity Sensors. *Materials* **2020**, *13* (2), 430.
(32) Zhao, Q.; Duan, Z.; Wu, Y.; Liu, B.; Yuan, Z.; Jiang, Y.; Tai, H. Facile Primary Battery-Based Humidity Sensor for Multifunctional Application. *Sens. Actuators, B* **2022**, *370*, 132369.
(33) Duan, Z.; Yuan, Z.; Jiang, Y.; Zhao, Q.; Huang, Q.; Zhang, Y.; Liu, B.; Tai, H. Power Generation Humidity Sensor Based on Primary Battery Structure. *Chem. Eng. J.* **2022**, *446*, 136910.
(34) Duan, Z.; Jiang, Y.; Tai, H. Recent Advances in Humidity Sensors for Human Body Related Humidity Detection. *J. Mater. Chem. C* **2021**, *9* (42), 14963−14980.
(35) Duan, Z.; Yuan, Z.; Jiang, Y.; Yuan, L.; Tai, H. Amorphous Carbon Material of Daily Carbon Ink: Emerging Applications in Pressure, Strain, and Humidity Sensors. *J. Mater. Chem. C* **2023**, *11* (17), 5585−5600.
(36) Li, Q.; Li, J.; Tran, D.; Luo, C.; Gao, Y.; Yu, C.; Xuan, F. Engineering of Carbon Nanotube/Polydimethylsiloxane Nanocomposites with Enhanced Sensitivity for Wearable Motion Sensors. *J. Mater. Chem. C* **2017**, *5* (42), 11092−11099.
(37) Jiménez-Suárez, A.; Campo, M.; Sánchez, M.; Romón, C.; Ureña, A. Influence of the Functionalization of Carbon Nanotubes on Calendering Dispersion Effectiveness in a Low Viscosity Resin for VARIM Processes. *Composites, Part B* **2012**, *43* (8), 3482−3490.
(38) Del Bosque, A.; Sánchez-Romate, X. F.; Sánchez, M.; Ureña, A.; Rey, U.; Carlos, J.; Tulipán, C. Easy-Scalable Flexible Sensors Made of Carbon Nanotube-Doped Polydimethylsiloxane: Analysis of Manufacturing Conditions and Proof of Concept. *Sensors* **2022**, *22* (14), 5147.
(39) Sánchez-Romate, X. F.; Artigas, J.; Jiménez-Suárez, A.; Sánchez, M.; Güemes, A.; Ureña, A. Critical Parameters of Carbon Nanotube Reinforced Composites for Structural Health Monitoring Applications: Empirical Results versus Theoretical Predictions. *Compos. Sci. Technol.* **2019**, *171*, 44−53.
(40) Simmons, J. G. Generalized Formula for the Electric Tunnel Effect between Similar Electrodes Separated by a Thin Insulating Film. *J. Appl. Phys.* **1963**, *34* (6), 1793−1803.
(41) Del Bosque, A.; Sánchez-Romate, X. F.; Sánchez, M.; Ureña, A. Wearable Sensors Based on Graphene Nanoplatelets Reinforced Polydimethylsiloxane for Human Motion Monitoring: Analysis of Crack Propagation and Cycling Load Monitoring. *Chemosensors* **2022**, *10* (2), 75.
(42) Jia, P.; Lu, J.; He, R.; Jiang, G.; Jiang, X.; Wang, B.; Song, L.; Hu, Y. Octopus Sucker-Inspired Hierarchical Structure MXene@carbon Nanotubes Enhancing the Mechanical Properties and Fire Safety of Thermoplastic Polyurethane Composites through the Interfacial Engineering. *Chem. Eng. J.* **2022**, *450*, 138184.
(43) Tas, M. O. O.; Baker, M. A.; Masteghin, M. G.; Bentz, J.; Boxshall, K.; Stolojan, V. Highly Stretchable, Directionally Oriented Carbon Nanotube/PDMS Conductive Films with Enhanced Sensitivity as Wearable Strain Sensors. *ACS Appl. Mater. Interfaces* **2019**, *11* (43), 39560−39573.
(44) Wang, Y.; Li, W.; Li, C.; Zhou, B.; Zhou, Y.; Jiang, L.; Wen, S.; Zhou, F. Fabrication of Ultra-High Working Range Strain Sensor Using Carboxyl CNTs Coated Electrospun TPU Assisted with Dopamine. *Appl. Surf. Sci.* **2021**, *566*, 150705.
(45) Shen, L.; Zhou, S.; Gu, B.; Wang, S.; Wang, S. Highly Sensitive Strain Sensor Fabricated by Direct Laser Writing on Lignin Paper with Strain Engineering. *Adv. Eng. Mater.* **2023**, *25*, 2201882.
(46) Li, Q.; Bai, R.; Gao, Y.; Wu, R.; Ju, K.; Tan, J.; Xuan, F. Laser Direct Writing of Flexible Sensor Arrays Based on Carbonized Carboxymethylcellulose and Its Composites for Simultaneous Mechanical and Thermal Stimuli Detection. *ACS Appl. Mater. Interfaces* **2021**, *13* (8), 10171−10180.
(47) Li, S.; Xu, R.; Wang, J.; Yang, Y.; Fu, Q.; Pan, C. Ultra-Stretchable, Super-Hydrophobic and High-Conductive Composite for Wearable Strain Sensors with High Sensitivity. *J. Colloid Interface Sci.* **2022**, *617*, 372−382.
(48) Zhou, J.; Long, X.; Huang, J.; Jiang, C.; Zhuo, F.; Guo, C.; Li, H.; Fu, Y. Q.; Duan, H. Multiscale and Hierarchical Wrinkle Enhanced Graphene/Ecoflex Sensors Integrated with Human-Machine Interfaces and Cloud-Platform. *npj Flexible Electron.* **2022**, *6* (1), 55.
(49) Tao, L. Q.; Wang, D. Y.; Tian, H.; Ju, Z. Y.; Liu, Y.; Pang, Y.; Chen, Y. Q.; Yang, Y.; Ren, T. L. Self-Adapted and Tunable Graphene Strain Sensors for Detecting Both Subtle and Large Human Motions. *Nanoscale* **2017**, *9* (24), 8266−8273.
(50) Shintake, J.; Piskarev, Y.; Jeong, H.; Floreano, D.; Shintake, J.; Jeong, S. H.; Floreano, D.; Piskarev, Y. Ultrastretchable Strain Sensors Using Carbon Black-Filled Elastomer Composites and Comparison of Capacitive Versus Resistive Sensors. *Adv. Mater. Technol.* **2018**, *3* (3), 1700284.
(51) Li, Y.; Zhou, B.; Zheng, G.; Liu, X.; Li, T.; Yan, C.; Cheng, C.; Dai, K.; Liu, C.; Shen, C.; Guo, Z. Continuously Prepared Highly Conductive and Stretchable SWNT/MWNT Synergistically Composited Electrospun Thermoplastic Polyurethane Yarns for Wearable Sensing. *J. Mater. Chem. C* **2018**, *6* (9), 2258−2269.
(52) Chen, J.; Li, H.; Yu, Q.; Hu, Y.; Cui, X.; Zhu, Y.; Jiang, W. Strain Sensing Behaviors of Stretchable Conductive Polymer Composites Loaded with Different Dimensional Conductive Fillers. *Compos. Sci. Technol.* **2018**, *168*, 388−396.
(53) Jeong, Y. R.; Park, H.; Jin, S. W.; Hong, S. Y.; Lee, S. S.; Ha, J. S. Highly Stretchable and Sensitive Strain Sensors Using Fragmentized Graphene Foam. *Adv. Funct. Mater.* **2015**, *25* (27), 4228−4236.

(54) Wang, Y.; Wang, S.; Li, M.; Gu, Y.; Zhang, Z. Piezoresistive Response of Carbon Nanotube Composite Film under Laterally Compressive Strain. *Sens. Actuators, A* **2018**, *273*, 140−146.
(55) Kuronuma, Y.; Takeda, T.; Shindo, Y.; Narita, F.; Wei, Z. Electrical Resistance-Based Strain Sensing in Carbon Nanotube/Polymer Composites under Tension: Analytical Modeling and Experiments. *Compos. Sci. Technol.* **2012**, *72* (14), 1678−1682.
(56) Lee, J. B.; Khang, D. Y. Electrical and Mechanical Characterization of Stretchable Multi-Walled Carbon Nanotubes/Polydimethylsiloxane Elastomeric Composite Conductors. *Compos. Sci. Technol.* **2012**, *72* (11), 1257−1263.
(57) Yang, H.; Yao, X. F.; Zheng, Z.; Gong, L. H.; Yuan, L.; Yuan, Y. N.; Liu, Y. H. Highly Sensitive and Stretchable Graphene-Silicone Rubber Composites for Strain Sensing. *Compos. Sci. Technol.* **2018**, *167*, 371−378.
(58) Li, W.; Zhou, Y.; Wang, Y.; Jiang, L.; Ma, J.; Chen, S.; Zhou, F. L. Core-Sheath Fiber-Based Wearable Strain Sensor with High Stretchability and Sensitivity for Detecting Human Motion. *Adv. Electron. Mater.* **2021**, *7* (1), 2000865.
(59) Hang, C. Z.; Zhao, X. F.; Xi, S. Y.; Shang, Y. H.; Yuan, K. P.; Yang, F.; Wang, Q. G.; Wang, J. C.; Zhang, D. W.; Lu, H. L. Highly Stretchable and Self-Healing Strain Sensors for Motion Detection in Wireless Human-Machine Interface. *Nano Energy* **2020**, *76*, 105064.
(60) Zhang, D.; Zhang, K.; Wang, Y.; Wang, Y.; Yang, Y. Thermoelectric Effect Induced Electricity in Stretchable Graphene-Polymer Nanocomposites for Ultrasensitive Self-Powered Strain Sensor System. *Nano Energy* **2019**, *56*, 25−32.
(61) Boutry, C. M.; Kaizawa, Y.; Schroeder, B. C.; Chortos, A.; Legrand, A.; Wang, Z.; Chang, J.; Fox, P.; Bao, Z. A Stretchable and Biodegradable Strain and Pressure Sensor for Orthopaedic Application. *Nat. Electron.* **2018**, *1* (5), 314−321.
(62) Qian, Q.; Wang, Y.; Zhang, M.; Chen, L.; Feng, J.; Wang, Y.; Zhou, Y. Ultrasensitive Paper-Based Polyaniline/Graphene Composite Strain Sensor for Sign Language Expression. *Compos. Sci. Technol.* **2019**, *181*, 107660.

https://doi.org/10.1021/acsapm.3c01689
ACS Appl. Polym. Mater. 2023, 5, 8589−8599